How well do we know thermal-NO? An investigation of NO formation in flames over a wide temperature range

Marie Meulemans[a,*], Antoine Durocher[a], Philippe Versailles[b]
Gilles Bourque[a,b], Jeffrey M. Bergthorson[a]

[a] *McGill University, 845 Sherbrooke St W, Montréal, QC H3A 0G4, Canada*
[b] *Siemens Energy Canada Limited, 9505 Chemin de la Côte-de-Liesse, Dorval, QC H9P 1A5, Canada*
∗*Corresponding author: marie.meulemans@mail.mcgill.ca*

June 25, 2022

Supplementary Material A: Experimentally-measured boundary conditions

Table S1 reports the experimental conditions used to perform simulations of quasi-1D stagnation flames.

Table S1: Flame boundary conditions

O_2-to-N_2*	X_{Ar}**	T_{ad} [K]	l [mm]	T_{in} [K]	u_{in} [ms^{-1}]	du/d$z|_{in}$ [s^{-1}]	T_{wall} [K]
0.21	0.0000	2130	7.12	291.3 ± 2	0.545 ± 0.001	156.4 ± 2.6	402.3 ± 5
0.21	0.1580	2000	7.09	290.6 ± 2	0.365 ± 0.001	91.2 ± 1.1	372.0 ± 5
0.21	0.2560	1900	7.10	291.1 ± 2	0.274 ± 0.001	57.3 ± 0.9	360.5 ± 5
0.40	0.6430	2000	7.43	291.7 ± 2	0.319 ± 0.001	81.7 ± 1.6	362.0 ± 5
0.40	0.6032	2100	7.26	291.4 ± 2	0.471 ± 0.001	121.1 ± 1.2	381.5 ± 5
0.40	0.5556	2200	7.30	291.4 ± 2	0.640 ± 0.001	175.2 ± 1.9	402.9 ± 5
0.40	0.4965	2300	6.91	292.0 ± 2	0.907 ± 0.002	245.7 ± 2.2	421.8 ± 5
0.40	0.4185	2400	6.91	291.9 ± 2	1.216 ± 0.002	333.9 ± 3.5	462.1 ± 5
0.40	0.3085	2500	6.84	291.9 ± 2	1.575 ± 0.003	472.7 ± 5.4	501.9 ± 5

* Defined in Eq. 1 of the main article; ** Defined in Eq. 2 of the main article

Supplementary Material B: Calibration of the optical constant C_{opt}

Following the NO-LIF methodology used for NO concentration measurements, as reported in Section 2 of the main article, the experimental signals of both a seeded flame and an unseeded flame, $F_{\mathrm{NO,exp}_{\mathrm{seeded}}}$ and $F_{\mathrm{NO,exp}_{\mathrm{unseeded}}}$ respectively, are collected. The seeding remains below 300ppm such that the consumption of seeded NO through the flame zone remains negligible [1]. The collected signals are subtracted from one another, such that the remaining signal $F_{\mathrm{NO,exp}_{\mathrm{net}}}$ is only proportional to the known concentration of NO ($n^{\circ}_{\mathrm{NO,known}}$):

$$F_{\mathrm{NO,exp}_{\mathrm{seeded}}} = F_{\mathrm{NO,exp}_{\mathrm{known}}} + F_{\mathrm{NO,exp}_{\mathrm{produced}}} \tag{1}$$

$$F_{\mathrm{NO,exp}_{\mathrm{unseeded}}} = F_{\mathrm{NO,exp}_{\mathrm{produced}}} \tag{2}$$

$$F_{\mathrm{NO,exp}_{\mathrm{net}}} = F_{\mathrm{NO,exp}_{\mathrm{seeded}}} - F_{\mathrm{NO,exp}_{\mathrm{unseeded}}} = F_{\mathrm{NO,exp}_{\mathrm{known}}} \tag{3}$$

Similar to the experiments, simulations are performed by virtually seeding the flame with an experimentally-known concentration of NO. The numerical NO profiles are transformed into LIF signal using the two-level LIF:

$$F_{\mathrm{NO,num}_{\mathrm{net}}} = C_{\mathrm{opt}} \cdot f_{\mathrm{LIF}}\left(f_{\mathrm{B}}, \lambda, \Delta\nu_{\mathrm{L}}, \Gamma, B_{12}, A_{21}, Q_{21}\right) \cdot n^{\circ}_{\mathrm{NO,known}} \tag{4}$$

where f_{LIF} is the number of photons emitted per unit molecule of NO, $f_{\mathrm{B}}(T)$ is the Boltzmann fraction of NO molecules in the excited state, λ is the laser wavelength, $\Delta\nu_{\mathrm{L}}$ is the spectral width of the laser, $\Gamma(\Delta\nu_{\mathrm{L}}, T, P, X_i)$ is the dimensionless overlap fraction, B_{12} is the Einstein constant of photon absorption, A_{21} is the rate constant of spontaneous emission, $Q_{21}(T, P, X_i)$ is the rate constant of non-radiative collisional quenching, and $n^{\circ}_{\mathrm{NO,known}}(T, P, X_{\mathrm{NO}})$ is the number density of NO molecules. Table S2 presents the LIF constants used to calculate the numerical NO-LIF signal.

Table S2: NO-LIF constants used the two-level LIF model in Eq. 4

Parameter	Function	Constants				Units
		c_1	c_2	c_3	c_4	
f_{B}	$c_1 e^{+c_2/T} + c_3 e^{+c4/T}$	-0.2822	-1799	0.2183	-408.4	[-]
λ_{on}		226.0345				[nm]
λ_{off}		226.047				[nm]
$\Delta\nu_{\mathrm{L}}$		0.25				[cm^{-1}]
Γ		0.86				[-]
B_{12}		$2.38{\cdot}10^{9}$				[$\mathrm{m}^2\mathrm{J}^{-1}\mathrm{s}^{-1}$]
A_{21}		$5.72{\cdot}10^{6}$				[s^{-1}]
Q_{21}	$\sum X_k Q_k$					[s^{-1}]
Q_k	$\sigma_k \left(\frac{N}{V}\right) \sqrt{\frac{8k_B T}{\pi \mu_k}}$					[s^{-1}]
μ_k	$\frac{m_k m_{\mathrm{NO}}}{m_k + m_{\mathrm{NO}}}$					[kg]
σ_k from [2]						[Å^2]

The direct comparison of $F_{\mathrm{NO,num_{net}}}$ and $F_{\mathrm{NO,exp_{net}}}$ allows the determination of the optical calibration coefficient (C_{opt}), by fitting the numerical and experimental profiles using a least-square fit. The calibration coefficient is fitted in the post-flame region, being the region of interest of this study. Figure S1 shows an example of the signal-fitting to obtain C_{opt}.

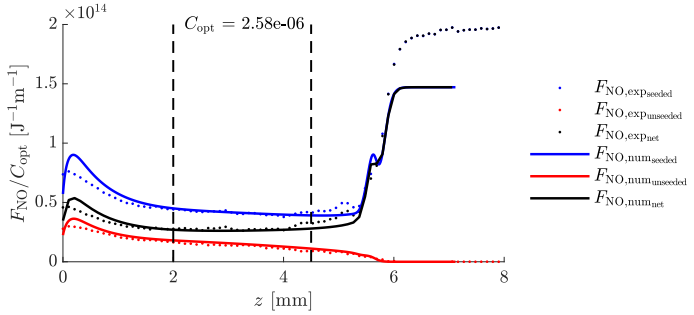

Fig. S1: Calibration obtained for the methane-air flame at T_{ad}=2130K with 50ppm seeding, using the GRI mechanism

The calibration has been performed approximately 50 times on different flame conditions and using different levels of seeding, leading to an average $\overline{C_{\mathrm{opt}}}$ of 2.56 $\cdot 10^{-6}$ m, as shown on Fig. S2. The coefficient has a low uncertainty ($\sim$2.90%) and confirms the independence of the seeding level and the flame condition on the calibration technique.

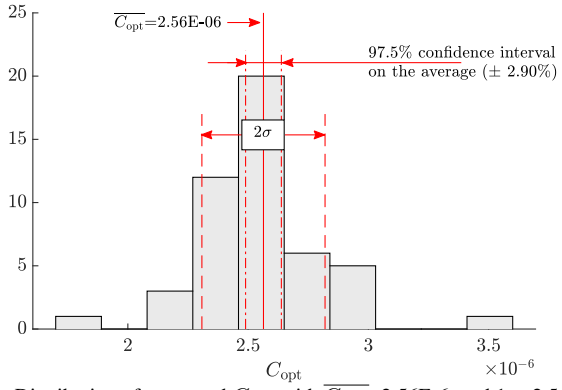

Fig. S2: Distribution of measured C_{opt}, with $\overline{C_{\text{opt}}}$=2.56E-6, and 1$\sigma$=2.56E-7.

Supplementary Material C: Uncertainty calculation

Total uncertainty of the NO slope ratio $\sigma_{\left(\mathrm{d}F_{\mathrm{NO,num}}/\mathrm{d}z\right)/\left(\mathrm{d}F_{\mathrm{NO,exp}}/\mathrm{d}z\right)=1}$, illustrated in Fig. 4, is a combination of the experimental and the numerical uncertainties. They are evaluated at the reference location z=3.5mm. The total uncertainty on the NO slope is thus defined as follows:

$$\sigma_{\left(\mathrm{d}F_{\mathrm{NO,num}}/\mathrm{d}z\right)/\left(\mathrm{d}F_{\mathrm{NO,exp}}/\mathrm{d}z\right)=1} = \left(\left(\overline{\sigma_{\mathrm{d}F_{\mathrm{NO}}/\left(C_{\mathrm{opt}}\cdot\mathrm{d}z\right)_{\text{exp,LIF}}}}\right)^2 + \left(\sigma_{\mathrm{d}F_{\mathrm{NO}}/\left(C_{\mathrm{opt}}\cdot\mathrm{d}z\right)_{\text{num,BC}}}\right)^2\right)^{1/2} \tag{5}$$

Numerical uncertainties

The numerical uncertainties represent the impact of the calculated boundary conditions on the numerical solutions. They are calculated by performing a brute-force sensitivity analysis of the numerical boundary conditions x_j on each of the simulated flames. The resulting logarithmic sensitivity L.S.(x_j) is weighted by the uncertainty of each of the boundary conditions parameters $\sigma(x_j)$ such that the impact on the NO slope $\mathrm{d}F_{\mathrm{NO}}/\left(C_{\mathrm{opt}}\cdot\mathrm{d}z\right)$ can be evaluated as follows:

$$\sigma_{\mathrm{d}F_{\mathrm{NO}}/\left(C_{\mathrm{opt}}\cdot\mathrm{d}z\right)_{\text{num,BC}}} = \left(\sum\left[\text{L.S.}(x_j)\cdot\sigma(x_j)\right]^2\right)^{1/2} \tag{6}$$

The logarithmic sensitivity for each parameter and each flame is shown in Fig. S3. One can see that the dilution of argon is the most sensitive boundary parameter on the slope of NO post-flame. As expected, a small change in X_{Ar} leads to a larger uncertainty for the most diluted flames, resulting in the largest numerical uncertainties for the flames at low temperature.

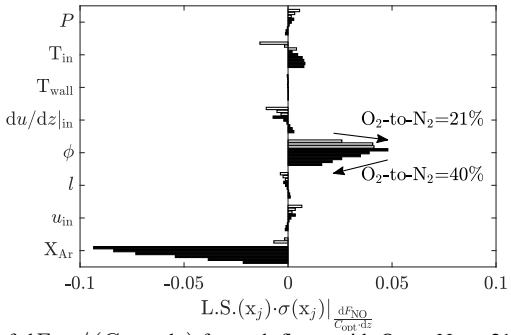

Fig. S3: Logarithmic sensitivity of $\mathrm{d}F_{\mathrm{NO}}/\left(C_{\mathrm{opt}}\cdot\mathrm{d}z\right)$ for each flame with O_2-to-N_2 = 21% (white) and O_2-to-N_2 = 40% (black). Increasing T_{ad} goes in the direction of the arrows.

Experimental uncertainty: NO-LIF

The experimental uncertainty $\sigma_{\mathrm{dNO/dz_{exp,LIF}}}$, for each profile, consists of the camera calibration coefficient uncertainty $\Delta C/C$, the image signal variation $\Delta S/S$, the laser energy variation $\Delta E_{\mathrm{L}}/E_{\mathrm{L}}$, the NO concentration calibration coefficient uncertainty $\Delta C_{\mathrm{opt}}/C_{\mathrm{opt}}$, and the NO profile linear regression uncertainty $\Delta f/f$, such that:

$$\sigma_{\mathrm{d}F_{\mathrm{NO}}/\left(C_{\mathrm{opt}}\cdot \mathrm{d}z\right)_{\mathrm{exp,LIF}}} = \left(\left(\frac{\Delta C}{C}\right)^2 + \left(\frac{\Delta S}{S}\right)^2 + \left(\frac{\Delta E_{\mathrm{L}}}{E_{\mathrm{L}}}\right)^2 + \left(\frac{\Delta C_{\mathrm{opt}}}{C_{\mathrm{opt}}}\right)^2 + \left(\frac{\Delta f}{f}\right)^2 \right)^{1/2} \tag{7}$$

Results presented in Fig. 4 have been averaged based on the sample size N_{s}, reducing the uncertainty as follows:

$$\overline{\sigma_{\mathrm{d}F_{\mathrm{NO}}/\left(C_{\mathrm{opt}}\cdot \mathrm{d}z\right)_{\mathrm{exp,LIF}}}} = \frac{\left\langle \sigma_{\mathrm{d}F_{\mathrm{NO}}/\left(C_{\mathrm{opt}}\cdot \mathrm{d}z\right)_{\mathrm{exp,LIF}}} \right\rangle_{1\rightarrow N_{\mathrm{s}}}}{\left(N_{\mathrm{s}}\right)^{1/2}} \tag{8}$$

This resulting uncertainty is applied on the averaged profiles shown in the NO-LIF figures of the article.

Supplementary Material D: Measured profiles

Figures S4-S6 show the measured profiles of Particle Tracking Velocimetry (PTV), Multi-line NO-LIF thermometry, and Planar LIF for the nine flames performed in this study.

Velocity measurements

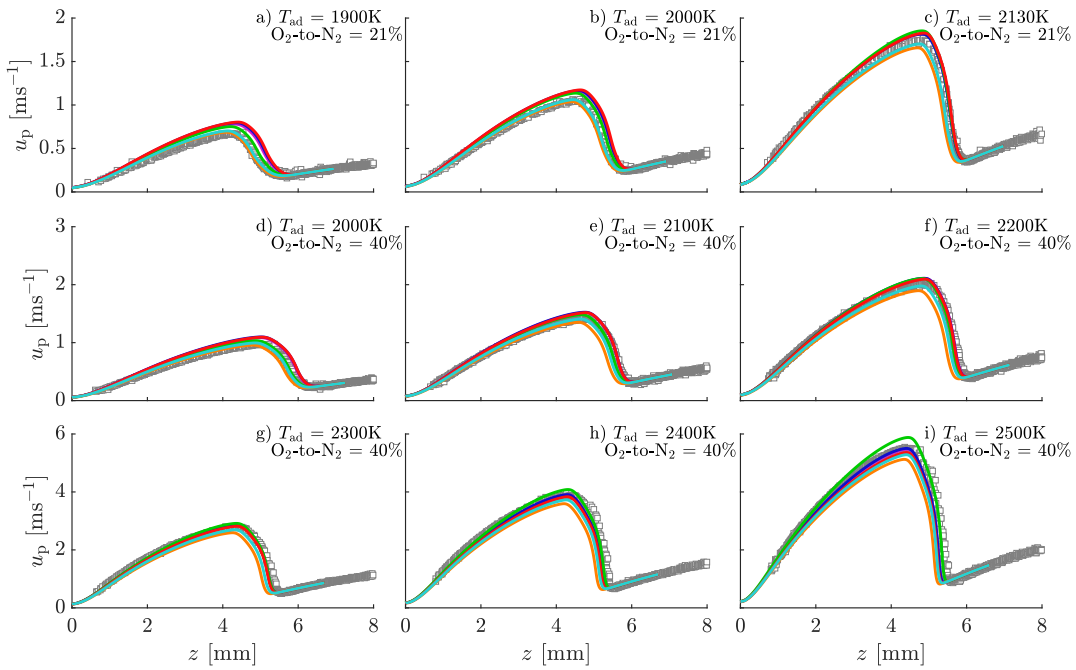

Fig. S4: Velocity profiles for methane-air-argon flames. Measured (□) and simulated (—) profiles are illustrated. Different thermochemical models are shown: GRI (—), SD (—), CRECK (—), NUIG (—), DTU (—) and KON (—).

Temperature measurements

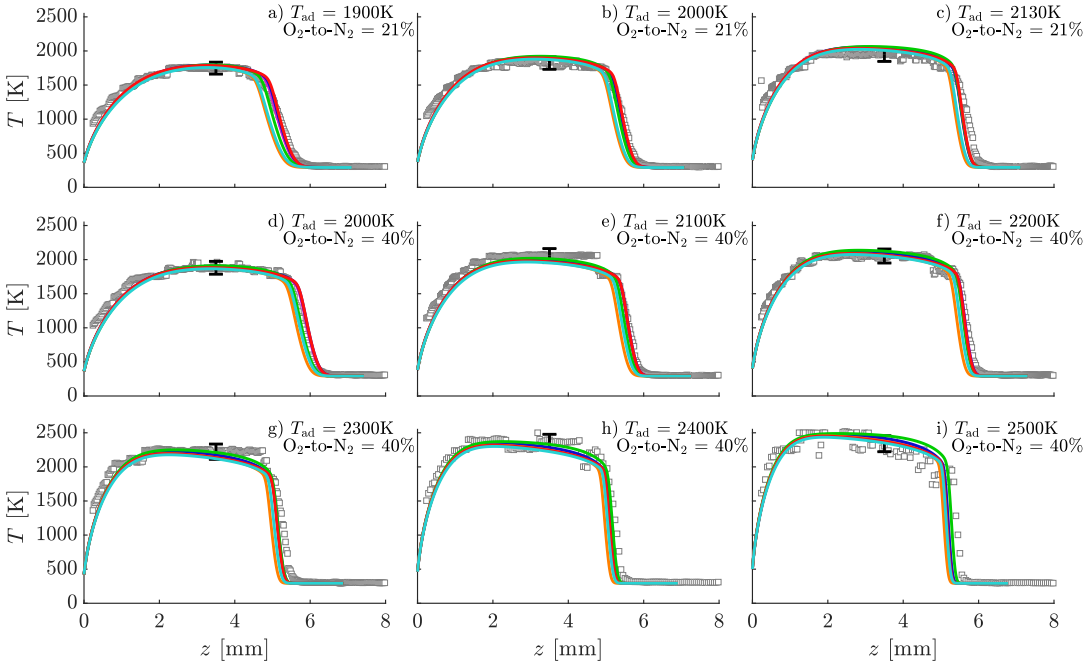

Fig. S5: Temperature profiles for methane-air-argon flames. Measured (□) and simulated (—) profiles are illustrated. Different thermochemical models are shown: GRI (—), SD (—), CRECK (—), NUIG (—), DTU (—) and KON (—).

NO-LIF measurements

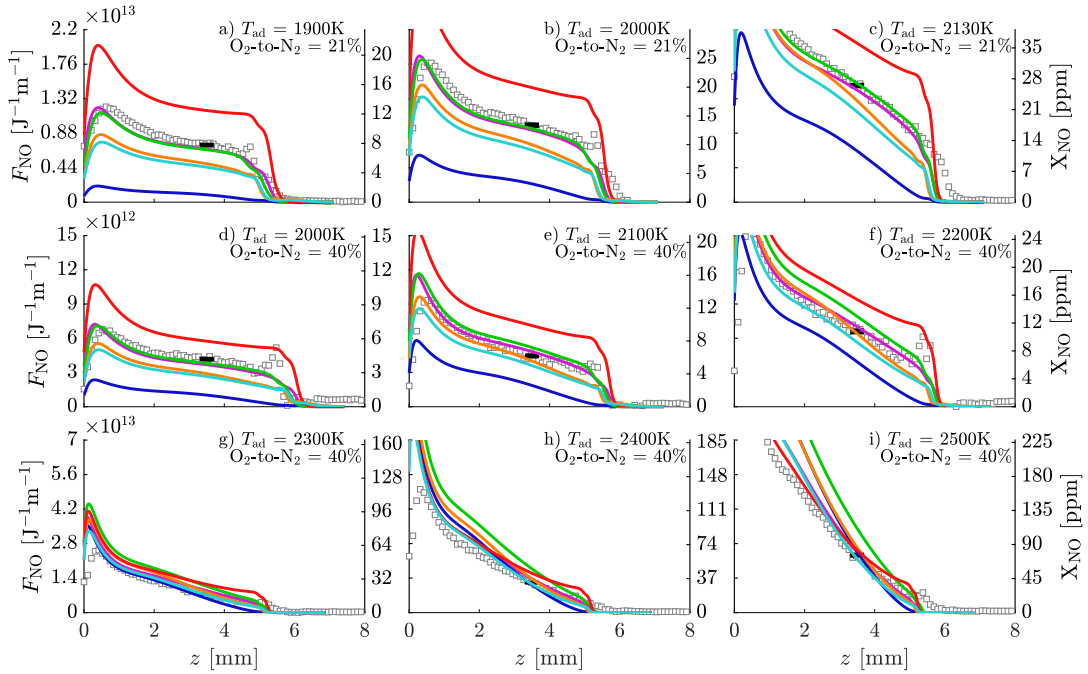

Fig. S6: NO profiles for methane-air-argon flames. Measured (□) and simulated (—) profiles are illustrated. Different thermochemical models are shown: GRI (—), SD (—), CRECK (—), NUIG (—), DTU (—) and KON (—).

References

[1] P. A. Berg, G. P. Smith, J. A. Y. B. Jeffries, D. R. Crosley, Nitric oxide formation and reburn in low-pressure methane flames (1998) 1377–1384.

[2] M. Tamura, P. A. Berg, J. E. Harrington, J. Luque, J. B. Jeffries, G. P. Smith, Collisional Quenching of CH(A), OH(A), and NO(A) in Low Pressure Hydrocarbon Flames, Combust. Flame 114 (1998) 502–514.